Environmental Science & Technology

pubs.acs.org/est

Article

Hexavalent Chromium Release in Drinking Water Distribution Systems: New Insights into Zerovalent Chromium in Iron Corrosion Scales

Cheng Tan, Sumant Avasarala, and Haizhou Liu*

Cite This: *Environ. Sci. Technol.* 2020, 54, 13036−13045

Read Online

ACCESS | Metrics & More | Article Recommendations | Supporting Information

ABSTRACT: Upon cast iron corrosion in contact with residual disinfectants, drinking water distribution systems have become potential geogenic sources for hexavalent chromium Cr(VI) release. This study investigated mechanisms of Cr(VI) release from cast iron corrosion scales. The oxidation of the corrosion scales by residual disinfectant chlorine released Cr(VI) and exhibited a three-phase kinetics behavior: an initial 2 h fast reaction phase, a subsequent 2-to-12 h transitional phase, and a final 7-day slow reaction phase approximately 2 orders of magnitude slower than the initial phase. X-ray absorption spectroscopy analysis discovered that zerovalent Cr(0) coexisted with trivalent Cr(III) solids in the corrosion scales. Electrochemical corrosion analyses strongly suggested that Cr(0) in the corrosion scales originated from Cr(0) in the cast iron alloy. Cr(0) exhibited a much higher reactivity than Cr(III) in the formation of Cr(VI) by chlorine. The presence of bromide in drinking water significantly accelerated Cr(VI) release because of its catalytic effect. Meanwhile, chlorine consumption was mainly attributed to the oxidation of organic matter and ferrous iron. Findings from this study point to a previously unknown but important pathway of Cr(VI) formation in drinking water, that is, direct oxidation of Cr(0) by chlorine, and suggest new strategies to control Cr(VI) in drinking water by inhibiting Cr(0) reactivity.

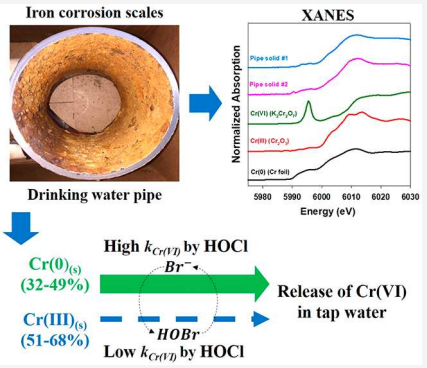

INTRODUCTION

Hexavalent chromium Cr(VI), typically existing as anion CrO_4^{2-} in drinking water, is acutely toxic and carcinogenic and listed as one high-priority contaminant by the U.S. EPA.[1] Exposure to Cr(VI) can cause lung cancer, liver damage, reproductive problems, and developmental harm.[2] U.S. EPA sets the maximum contaminant level for total Cr at 100 μg/L.[3] A health guideline of 0.02 μg/L for Cr(VI) was issued by the Office of Environmental Health Hazard Assessment in California.[4] A Cr(VI) drinking water standard at 10 μg/L was also established in California in 2014 that was later withdrawn because of the lack of economically feasible treatment.[5,6] As new cost-effective treatment technologies emerge, a new Cr(VI) regulation will be reconsidered in the future.[7,8]

In order to control Cr(VI) occurrence in tap water, it is critical to identify the main sources of Cr(VI). Even with adequate drinking water treatment prior to the entry point of the distribution systems, the Cr(VI) level at the consumers' tap water may increase resulting from reactions taking place in the distribution systems.[9,10] Analysis of the U.S. EPA nationwide Cr(VI) monitoring database shows that there was a 41% chance for an increase in the Cr(VI) concentration in distribution systems, and the increase was strongly correlated with the presence of free chlorine as the residual disinfectant.[11] Cr(III) solids predicted to exist in corrosion scales, including $Cr(OH)_{3(s)}$, $Cr_2O_{3(s)}$, $Cu_2Cr_2O_{5(s)}$, and $Fe_xCr_{1-x}(OH)_{3(s)}$, can be oxidized by chlorine and release Cr(VI).[12,13] Despite the importance of corrosion scales to Cr(VI) release control, no study has directly investigated the fate of Cr in naturally formed corrosion scales from drinking water distribution systems (DWDSs). As a result, there lacks a clear understanding on the oxidation states of Cr in corrosion scales and the mechanisms of Cr(VI) release during drinking water distribution.

The formation of Cr(III) solids in corrosion scales is traditionally believed to result from reductive sequestering of Cr(VI) from source water.[11−13] Meanwhile, a zerovalent chromium material is intrinsically present in DWDSs; it is an additive in cast iron and ductile iron pipe alloys to resist corrosion. For example, corrosion−resistant cast iron consists 12−18% of mass as zerovalent chromium.[14] However, little is known about the fate of zerovalent Cr and its reactivity as cast iron pipes corrode.

Received: June 16, 2020
Revised: September 1, 2020
Accepted: September 2, 2020
Published: September 30, 2020

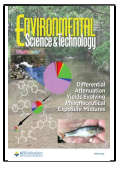

Furthermore, the iron corrosion scales are rich in reductants including organic matter and ferrous iron Fe(II).[15,16] Organic carbon was among the most abundant components of the corrosion scales with a median concentration of 9.8 mg/g.[15] Its sources are from the biofilm grown on the surface of corrosion scales and sorption of natural organic matter (NOM) present in source waters. Ferrous solids including ferrous hydroxide $Fe(OH)_{2(s)}$, wustite $FeO_{(s)}$, siderite $FeCO_{3(s)}$, and magnetite $Fe_3O_{4(s)}$ were found in the iron corrosion scales.[16] Organic matter and Fe(II) solids can compete with Cr components for chlorine.[17−19] However, little is known about the contributions of Fe(II) and organic matter on the consumption of chlorine and associated effects on the release of Cr(VI) from iron corrosion scales.

Previous water crises in Flint, Michigan, and Washington, DC highlight the urgency to better understand the potential risks of metal release due to changes of water chemistry.[20,21] In the future, efforts to fight water scarcity will incorporate more reclaimed and desalinated water as new drinking water sources into existing distribution systems.[22] Higher bromide levels in these alternative water resources can catalyze the oxidation of Cr(III) solids by chlorine.[12,13] To what extent bromide will increase the release of Cr(VI) from naturally formed iron corrosion scales needs better understanding. Overall, a thorough understanding of the mechanisms of Cr(VI) release from iron corrosion scales is needed to develop control strategies regarding the drinking water distribution infrastructure.

Accordingly, the objectives of this study were to understand the speciation of chromium in the cast iron corrosion scales, investigate the kinetics of Cr(VI) release by chlorine via the oxidation of iron corrosion scales, examine the catalytic effect of bromide, and quantify the potential contribution of Cr(0) in cast iron pipes to the formation of Cr(VI) in drinking water.

MATERIALS AND METHODS

Preparation of Iron Corrosion Scales and Cr Reference Solids. Two cast iron pipe sections (labeled as pipe #1 and pipe #2) with contrasting Cr(VI) levels in their drinking water sources were collected from DWDSs at two U.S. West Coast states (Figure S1 in the Supporting Information section). Pipe #1 was in service for 5 years and collected from a distribution system using groundwater as the source water. Historical Cr(VI) concentrations in the groundwater water were very high, ranging between 11 and 24 μg/L (Table 1). In contrast, pipe #2 was in service for approximately 70 years and collected from a distribution system using surface water as the source water, in which Cr(VI) was nondetectable (Table 1). To obtain pipe corrosion scale solids, corrosion scales with approximately 1 cm in depth from the surface were first scratched off from eight different locations on the inner surface of one pipe section, and then, they were mixed together in equal weights as one composite corrosion solid sample. After grinding and sieving, homogenized corrosion products with particle sizes between 45 and 90 μm were used in this study (labeled as pipe solid #1 and pipe solid #2, respectively). Corrosion scales were only collected within 1 cm depth from the surface in order to represent the corrosion scales directly in contact with drinking water in the distribution systems as much as possible. Furthermore, a previous study showed that electrons from the inside pipe material can be conducted through the scale to a site on the surface of iron corrosion scales, which means that direct contact between free chlorine

Table 1. Background Information and Characteristics of the Iron Corrosion Scales Used in This Study

	history of pipe section			naturally formed iron corrosion scales							freshly produced iron corrosion scales		
	service time (years)	source water	Cr(VI) in source water (μg/L)	pH_{pzc}	surface area (m^2/g)	Fe_{TOT} (g/g)	Fe(II)(g/g)	Fe(III)(g/g)	Cr_{TOT} (μg/g)	Cr(0) (μg/g)	Cr(III) (μg/g)	Cr_{TOT} (μg/g)	Cr(0) (μg/g)	Cr(III) (μg/g)
pipe #1	5	groundwater	11−24	7.9	96.1	0.51	0.03 ± 0.01	0.48 ± 0.01	1333 ± 82	653 ± 40	680 ± 42	652 ± 23	609 ± 18	43 ± 5.0
pipe #2	70	surface water	non-detectable	7.9	95.7	0.52	B.D.	0.52	74 ± 5.8	24 ± 1.9	50 ± 3.9	75 ± 5.2	27 ± 1.1	48 ± 4.1

https://dx.doi.org/10.1021/acs.est.0c03922
Environ. Sci. Technol. 2020, 54, 13036−13045

and Cr(0) on the surface of the corrosion scales is not necessary for the oxidation of Cr(0) with free chlorine as long as a path exists for electron movement.[23] Therefore, it is possible that some Cr solids close to the surface layer of iron corrosion scales could be oxidized with chlorine even without direct contact. Although homogenization could alter the structure of the iron corrosion scales, the use of homogenized iron corrosion solids provides a standardized solid material to understand the fundamental mechanisms of Cr(VI) formation during the oxidation of the corrosion scales. Surface and bottom layers of corrosion scales were also collected from the 1 cm depth by carefully cutting them off from the corroded pipe inner surfaces. Three Cr(III)−Fe(III) hydroxide solids with varying Cr molar ratios, that is, $Fe_{0.25}Cr_{0.75}(OH)_{3(s)}$, $Fe_{0.5}Cr_{0.5}(OH)_{3(s)}$, and $Fe_{0.75}Cr_{0.25}(OH)_{3(s)}$, were synthesized using a standard protocol and used as the trivalent Cr(III) reference solids.[24] After grinding and sieving, the Cr(III)−Fe(III) hydroxide solids with particle sizes between 45 and 90 μm were used. Cr(0) powder of 45 μm purchased from Sigma-Aldrich was used as the zerovalent Cr(0) reference solid. Chlorine stock solution (HOCl) was prepared freshly using a NaOCl solution, and the bromine stock solution (HOBr) was prepared by adding NaBr into NaOCl stock solution with 10% access of Br^-.[13]

Oxidation Experiments with Iron Corrosion Scales and Reference Solids. To start a 7-day oxidation experiment between a solid and oxidant, 20 g/L suspension of a pipe corrosion scale solid or 10 mg/L suspension of a reference solid was mixed with 200 mg Cl_2/L (equivalent of 2.8 mM) of HOCl or HOBr in a 250 mL glass vessel in darkness. The choice of an oxidant concentration higher than 2 mg Cl_2/L in these experiments did not change the redox ladder compared to that in drinking water conditions and provides valuable insight into the oxidation kinetics, a technique used in prior studies.[12,13,25,26] Because bromide reacts instantaneously with HOCl to form HOBr,[27] HOBr was directly used to understand the bromide effect on the oxidation of iron corrosion scales by chlorine, a technique also used in prior studies.[26] The pH of the suspension was maintained at 7 ± 0.1 throughout the reaction with a Eutech Instrument Alpha pH200 controller. At each time point, 0.2 mL of suspension was collected, filtered through 0.22 μm filters, and diluted by 100 times to measure the HOCl or HOBr concentration, and additional HOCl or HOBr was added into the reactor to adjust its concentration back to 200 mg Cl_2/L. In addition, 5 mL of suspension was collected, quenched by adding excess $(NH_4)_2SO_4$, adjusted pH to 8.5, and filtrated by 0.22 μm filters. The concentrations of total Cr, Cr(VI), and dissolved organic carbon (DOC) in the filtrates were measured. Fe(II) concentrations in the iron corrosion solids were quantified.

To understand the accumulation of chromium in the corrosion scales due to iron corrosion, fresh iron corrosion scales were produced by electrochemically corroding a fresh surface of each cast iron pipe using an electrochemical station (Pine Instrument Inc., Durham, NC). One piece of 7.6 cm × 7.6 cm plates from each cast iron pipe was cut and sanded until the fresh metal surface was exposed on all sides. Following that, this plate was used as the anode, submerged in deionized (DI) water at pH 7, and applied with a constant voltage of 2 V for 7 days with a platinum electrode as the cathode. After that, corrosion scale samples collected from the corroded fresh metal plate were freeze-dried, ground into powder, and sieved to obtain the homogenized corrosion solids with particle sizes between 45 and 90 μm.

Analytical Methods. The concentration and redox speciation of Cr and Fe in pipe corrosion solids were characterized by X-ray absorption spectroscopy (XAS) at the Stanford Synchrotron Radiation Laboratory. Powder samples of mixed corrosion solids and sheet samples of surface and bottom corrosion layers were analyzed at beamlines 4−3 and 10−2, respectively. The radiation was monochromatized using a Si(220) double-crystal monochromator. Samples were measured in the transition mode with a N_2-filled ionization chamber. Two to three scans were recorded for each sample to ensure reproducibility. All measurements were carried in the transmission mode. The X-ray energy was varied from 50 eV below to 150 eV above the absorption K-edge of Fe (7112 eV) and Cr (5989 eV). The oxidation states of Cr in the iron corrosion scales were obtained by linear combination fitting (LCF) of the Cr X-ray absorption near edge structure (XANES) spectra using reference spectra of Cr(0), Cr(III), and Cr(VI) standard solids.

The Brunauer−Emmett−Teller (BET) surface area of iron corrosion scale solids was measured using a Micromeritics ASAP 2020 surface area analyzer. The concentration of Cr(III) in the pipe corrosion solids was quantified using the EPA acid digestion method 3050B.[28] This standard method can reliably quantify Cr(III) without inference from Cr(0), with a recovery of 106 ± 6.5% using the Cr(III) reference solid $Fe_{0.75}Cr_{0.25}(OH)_{3(s)}$ and a negligible recovery using the Cr(0) reference solid (Figure S2). Because the EPA acid digestion can dissolve all the Cr(III) reference solids and Cr(0) had a very low surface area of 0.055 m^2/g, the quantification of Cr(VI) should not be affected by the adsorption of Cr(VI) on Cr solids. The concentration of total Cr in the pipe corrosion solids was measured using a bromine digestion subsequent to EPA acid digestion. Briefly, the EPA method digested solution was mixed with 620 mM of bromine solution and further digested at 95 °C for 6 h. The bromine concentration was maintained during the digestion by manually adding extra bromine if necessary. After the bromine digestion, the total dissolved Cr was measured, and Cr(0) in the iron corrosion scales was calculated based on mass balance between total Cr and Cr(III). The bromine digestion method achieved a Cr(0) recovery of 94 ± 3.3% using the reference Cr(0) solid (Figure S2). The speciation of Fe(II) and Fe(III) in the pipe corrosion solids was calculated based on the mass concentration of total Fe and the fractions of Fe(II) and Fe(III) obtained from the XANES analysis. The concentrations of total dissolved Cr and total dissolved Fe in the digested samples and in the filtered samples from oxidation experiments were analyzed using Agilent 7700 inductively coupled plasma mass spectrometry. The Cr(VI) concentration in the samples was measured using the standard diphenylcarbazide method.[29] The values of the reaction rate constant of Cr(VI) formation ($k_{Cr(VI)}$) were obtained by fitting experimental data with the kinetics model using software OpenModel. HOCl or HOBr concentrations were measured by using the standard DPD method.[29] The DOC was analyzed by a total organic carbon analyzer (Aurora 1030C). Fe(II) fractions in the iron corrosion scales during oxidation experiments were extracted using 9 M HCl for 2 h[30] The Fe(II) level was analyzed by using the standard phenanthroline method.[29]

https://dx.doi.org/10.1021/acs.est.0c03922
Environ. Sci. Technol. 2020, 54, 13036−13045

RESULTS AND DISCUSSION

Solid Phase Characterization of Iron Corrosion Scales. The two iron corrosion scales from geographically different locations have very similar physical-chemical characteristics except for different Cr cumulation levels. They had identical surface areas of 96 m^2/g and a point of zero charge (pH_{pzc}) of 7.9 (Table 1 and Figure S3). The pH_{pzc} was very similar to that of ferrihydrite (7.6−8.5),[31,32] indicating that ferrihydrite was likely the dominant Fe species in the corrosion scales. The reference Cr(III)−Fe(III) hydroxide solids had comparable surface areas of 198−355 m^2/g to the iron corrosion scales. In contrast, the reference Cr(0) solid had a much lower surface area of 0.055 m^2/g because of the smooth surface of metallic Cr. The Cr concentration in pipe solid #1 was 1333 ± 82 $\mu g/g$, approximately 18 times higher than that in pipe solid #2 (74 ± 5.8 $\mu g/g$). These Cr concentrations are consistent with the Cr concentrations in deposit samples in DWDSs reported in a prior study.[33] The dominant element in these two corrosion scales was iron, which accounted for approximately 50% mass of the corrosion scales (Table 1). Because the Cr concentration in pipe solid #1 was significant, additional XAS mapping on the surface layer (exposed to drinking water) and bottom layer (attached to pipe inner surface) of the intact corrosion scales from pipe #1 was conducted. The mapping showed that Cr existed both in the surface layer and the bottom layer of iron corrosion scales (Figures 1A and S4). The image mapping analysis also showed Cr correlated with Fe in both layers (Figure S5), indicating that Fe and Cr mixed phase solids such as $Fe_xCr_{(1-x)}(OH)_{3(s)}$ likely existed in the iron corrosion scales.[34,35]

XANES spectra of corrosion solids showed that chromium existed in two oxidation states of Cr(0) and Cr(III) in pipe corrosion solids (Figure 1B). LCF analysis of the spectra showed that a substantial amount of Cr(0) existed in both corrosion scales, accounting for 49 ± 4.7 and 32 ± 4.2% of total Cr for solid #1 and solid #2, respectively. In addition, based on LCF analysis of the Fe XANES spectra (Figure S6), a majority of iron existed as Fe(III) in the corrosion solids (Table 1).

Kinetics of Oxidative Cr(VI) Release by Chlorine and Bromine. Oxidation experiments show that the Cr(VI) release kinetics followed a nonlinear pattern with three distinct phases: an initial fast phase of Cr(VI) release within the first 2 h, a second transitional phase of Cr(VI) release from 2 to 12 h, and a final slow phase of Cr(VI) release lasting for 7 days (Figure 2). In contrast, in the controls without any oxidant, no Cr(VI) leached out from the corrosion scales. This trend supports that Cr(VI) release from iron corrosion scales was driven by the oxidative conversion of Cr sources via HOCl and HOBr. For example, after 2 h of reaction, the Cr(VI) release from pipe solid #1 increased dramatically from nondetectable to 1.1 and 1.9 mg/L in the presence of HOCl and HOBr, respectively (insets of Figure 2A,B), and further slowly increased to 2.7 and 2.8 mg/L after 7 days of reaction, respectively (Figure 2A,B). Pipe solid #1 exhibited a cumulative Cr(VI) release approximately 12−13 times higher than solid #2 (Figure 2A *vs* 2B) mainly because of a significant difference in total Cr accumulation in these solids. In addition, chromium released from the corrosion scales only existed as Cr(VI), as shown by the same Cr(VI) and total Cr levels in the solution (Figure S7).

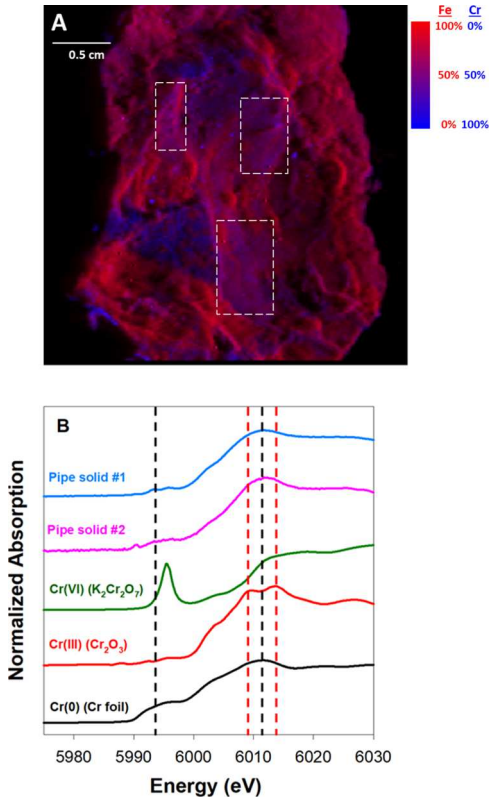

Figure 1. XAS characterization of iron corrosion scales. (A) Mapping of Cr and Fe in the bottom layer of the iron corrosion scales from pipe #1 (pink color represents the coexistence of Cr (blue) and Fe (red), and some spots of coexistence of Cr and Fe were indicated in white rectangles); and (B) Cr K-edge XANES of reference solids and the pipe solids [the black and red dashed lines represent the post-K edge features of Cr(0) and Cr(III)].

A second-order reaction kinetics model was introduced to quantify the reaction rate constant of Cr(VI) formation ($k_{Cr(VI)}$) based on eq 1

$$\frac{d[Cr(VI)]}{dt} = k_{Cr(VI)}[Cr_{(s)}][oxidant](S_{Cr_{(s)}})(AW_{Cr}) \quad (1)$$

where $k_{Cr(VI)}$ is the surface-area normalized second-order rate constant for Cr(VI) formation from corrosion scales or the reference Cr solid ($L \cdot m^{-2} \cdot min^{-1}$), either driven by HOCl or HOBr. [Oxidant] is the HOCl or HOBr concentration (mol/L), $[Cr_{(s)}]$ is the reactive Cr concentration (mol/L). $S_{Cr_{(s)}}$ is the Cr-containing solid BET surface area (m^2/g), and AW_{Cr} is the Cr atomic weight of (52 g/mol). $[Cr_{(s)}]$ and [oxidant] are variables, and $k_{Cr(VI)}$, $S_{Cr_{(s)}}$, and AW_{Cr} are constants. $[Cr_{(s)}]$ equaled to the initial Cr solid minus formed dissolved Cr(VI) at time *t*. All the measured [Cr(VI)] and [oxidant] at different time points were used in the model to fit $k_{Cr(VI)}$. For the iron corrosion scales, $k_{Cr(VI)}$ was fitted in three phases, that is, an initial fast phase (0−2 h), a transitional phase (2−12 h), and a slow phase (0.5−7 days). For the Cr reference solids, $k_{Cr(VI)}$ was fitted in one phase. All fitting curves well-matched the observed Cr(VI) concentrations with R^2 ranging between 0.981 and 0.998 (detailed fitting data shown in Figures S8 and S9).

For both iron corrosion scales, the $k_{Cr(VI)}$ values with HOCl decreased significantly as the reaction time proceeded (Figure 3). In the first phase (0−2 h), the $k_{Cr(VI)}$ values of corrosion

https://dx.doi.org/10.1021/acs.est.0c03922
Environ. Sci. Technol. 2020, 54, 13036−13045

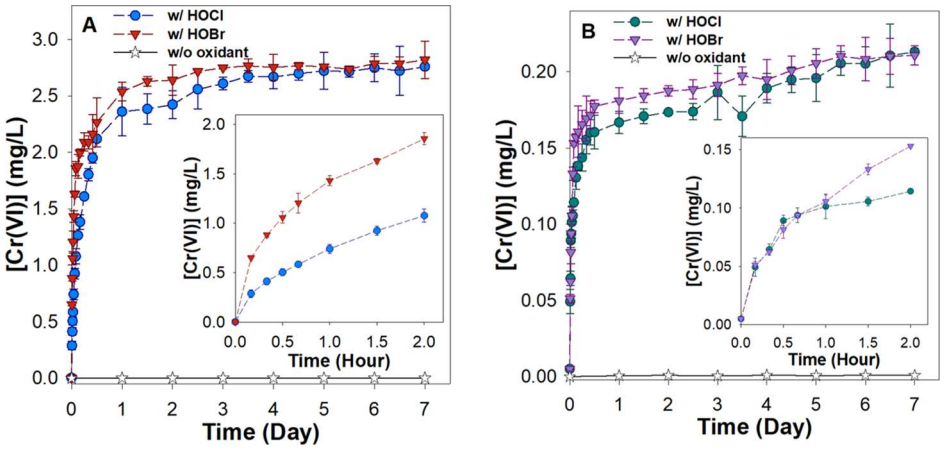

Figure 2. Dissolved Cr(VI) concentrations for 7 days of oxidation of pipe solids from two cast iron pipes in drinking water distribution systems with oxidants. [Pipe corrosion solid] = 20 g/L; [HOCl] = 200 mg Cl_2/L (2.8 mM); [HOBr] = 200 mg Cl_2/L (2.8 mM), pH = 7 (A) pipe solid #1; (B) pipe solid #2.

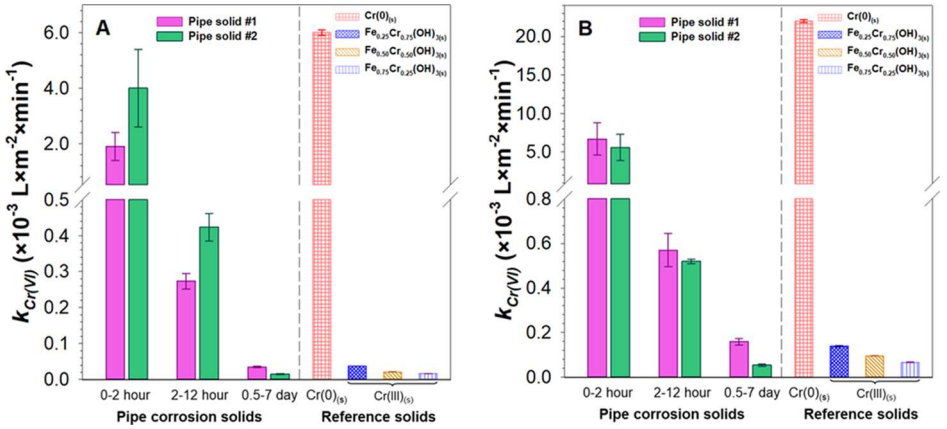

Figure 3. Surface area normalized second-order Cr(VI) formation rate constants of pipe solids and reference Cr(III) and Cr(0) solids. (A) Reaction with HOCl and (B) reaction with HOBr.

scales were 1.9×10^{-3} and 3.9×10^{-3} L·m^{-2}·min^{-1} with HOCl for solid #1 and solid #2, respectively (Figure 3A). These $k_{Cr(VI)}$ values were more than 1 order of magnitude higher than those of trivalent Cr(III) reference solids (Figure 3A). Therefore, the fast Cr(VI) formation cannot be explained by the oxidation of Cr(III) solids in corrosion scales.[12,13] In contrast, the zerovalent Cr(0) reference solid had an extremely higher $k_{Cr(VI)}$ with HOCl compared to Cr(III) reference solids (6×10^{-3} *vs* 1.6–3.7×10^{-5} L·m^{-2}·min^{-1}, Figure 3A). The $k_{Cr(VI)}$ values of pipe corrosion solids during the first 2 h were very similar to the $k_{Cr(VI)}$ value of Cr(0) powder during oxidation with HOCl. Given that the oxidant decay induced by Fe(III) surface sites in the pipe corrosion solids may interfere the reaction between Cr(0) and the oxidant,[13] the observed $k_{Cr(VI)}$ values of pipe solids were slightly lower than those of the pure Cr(0) reference solid. Thermodynamics calculation showed that the redox potential of Cr(VI)/Cr(0) is lower than that of HOCl/Cl$^-$, thus the oxidation of Cr(0) by HOCl is thermodynamically feasible (Text S1 and Table S1), Therefore, the oxidation of the zerovalent Cr(0) solid in the iron corrosion scales was the dominant reaction during the first 2 h of reaction as descripted below, and it resulted in the fast Cr(VI) release

$$Cr_{0(s)} + 3HOCl + H_2O \rightarrow CrO_4^{2-} + 5H^+ + 3Cl^- \quad (2)$$

During the third phase of the reaction (0.5–7 days), the $k_{Cr(VI)}$ values were 4.0×10^{-5} and 1.4×10^{-5} L·m^{-2}·min^{-1} with HOCl for solid #1 and solid #2, respectively. All these $k_{Cr(VI)}$ values in the third phase well-matched with the $k_{Cr(VI)}$ of Cr(III) reference solids $Fe_xCr_{(1-x)}(OH)_{3(s)}$ in this study (Figure 3A). The $k_{Cr(VI)}$ values by HOCl in the third phase were also very similar to the previously reported $k_{Cr(VI)}$ of other Cr(III) solids ($Cr(OH)_{3(s)}$, $Cr_2O_{3(s)}$, and $Cu_2Cr_2O_{5(s)}$) by HOCl.[12] Thermodynamics calculation also showed that the redox potential of Cr(VI)/Cr(III) is lower than the HOCl/Cl$^-$ couple (Text S1 and Table S1). Therefore, the slow Cr(VI) release process from 0.5 to 7 days was due to the oxidation of Cr(III) solids in the iron corrosion scales as described below

$$2Cr_{(III)(s)} + 3HOCl + 5H_2O \rightarrow 2CrO_4^{2-} + 13H^+ + 3Cl^- \quad (3)$$

The second transition phase (2–12 h) started from the oxidation of Cr(0) solid as the dominant reaction and ended with the oxidation of the Cr(III) solid as the dominant reaction. As the concentration of Cr(0) in the corrosion solid decreased, the formation of Cr(VI) decreased with time. Overall, the formation of Cr(VI) depended on both the oxidation of Cr(0) and Cr(III) solids in this transition phase. The same trend was also observed during HOBr-driven oxidation, except that the $k_{Cr(VI)}$ values were 1.3–4.3 times

https://dx.doi.org/10.1021/acs.est.0c03922
Environ. Sci. Technol. 2020, 54, 13036–13045

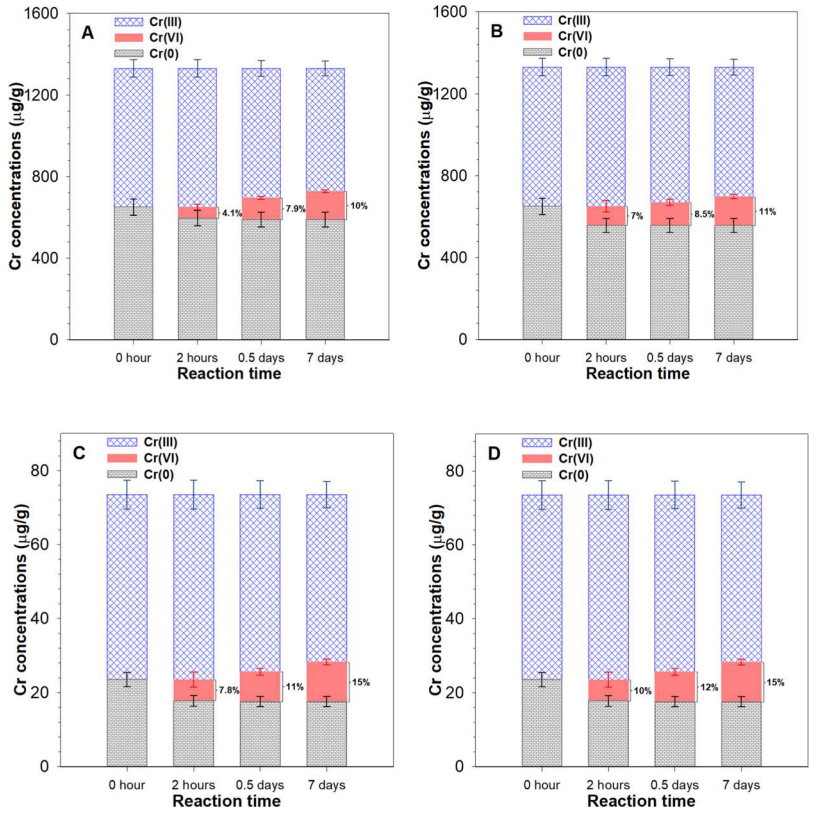

Figure 4. Contributions of Cr(0) and Cr(III) solids on Cr(VI) formation calculated based on the 7 days of oxidation reaction. (A) Pipe solid #1 with HOCl; (B) pipe solid #1 with HOBr; (C) pipe solid #2 with HOCl; and (D) pipe solid #2 with HOBr.

higher than those in HOCl-driven oxidation (Figure 3A *vs* 3B). For instance, in the initial fast phase (0−2 h), the $k_{Cr(VI)}$ was 6.6×10^{-3} L·m^{-2}·min^{-1} with HOBr versus 1.9×10^{-3} L·m^{-2}·min^{-1} with HOCl for solid #1 and was 5.6×10^{-3} L·m^{-2}·min^{-1} with HOBr versus 3.9×10^{-3} L·m^{-2}·min^{-1} with HOCl for solid #2 (Figure 3A *vs* 3B). For all reference Cr(0) and Cr(III) solids, the values of $k_{Cr(VI)}$ with HOBr were 3.7−4.5 times higher than that with HOCl (Figure 3A *vs* 3B). HOBr is more electrophilic than HOCl, and HOBr exhibited a faster kinetics in oxidizing electron-rich transition metals and organic matter.[27] HOBr-driven oxidation takes place when bromide is present in the HOCl system

$$HOCl + Br^- \rightarrow HOBr + Cl^- \quad (4)$$

$$Cr_{0(s)} + 3HOBr + H_2O \rightarrow CrO_4^{2-} + 5H^+ + 3Br^- \quad (5)$$

$$2Cr_{(III)(s)} + 3HOBr + 5H_2O \rightarrow 2CrO_4^{2-} + 13H^+ + 3Br^- \quad (6)$$

Essentially bromide acts as an electron shuttle to catalyze the oxidation of both Cr(0) and Cr(III) by HOCl.

The contributions of Cr(0) and Cr(III) solids on the formation of Cr(VI) were calculated (Figure 4) (in the first phase $\Delta[Cr(VI)] = -\Delta[Cr(0)]$; in the second phase $\Delta[Cr(VI)] = -\Delta[Cr(0)] - \Delta[Cr(III)]$ and $\Delta[Cr(III)] = -k_{Cr(VI)(3rd\ phase)}[Cr_{(III)(s)}][oxidant](S_{Cr_{(s)}})\cdot(AW_{Cr})\cdot(t)$; and in the third phase $\Delta[Cr(VI)] = -\Delta[Cr(III)]$). Initially, there was no Cr(VI) in the iron corrosion scales. After 2 h of reaction with HOCl or HOBr, 4.1−10% of the total Cr was oxidized to Cr(VI) assuming that only the oxidation of Cr(0) solids occurred. From 2 to 12 h, the oxidation of Cr(0) and Cr(III) solids together resulted in oxidation of an additional of 1.5−3.8% of the total Cr to Cr(VI). From 0.5 to 7 days, Cr(III) solids accounting for 2.1−4% of the total Cr were oxidized to Cr(VI). However, after 7 days of reaction, only 10−15% of the total Cr in solids was oxidized to Cr(VI) and released in water, and significant amounts of Cr(0) solids were still in both iron corrosion scales (Figure 4). The inactivation of Cr(0) after 2 h of reaction may result from the formation of a thin passivation Cr(III) layer that insulates Cr(0) from further interacting with the oxidant. It was reported previously that a Cr(III) $Cr_2O_{3(s)}$ layer formed on the Fe−Cr alloys inhibiting its further oxidation because the Cr(III) $Cr_2O_{3(s)}$ layer is much more dense and less porous than iron oxide, and it is efficient to inhibit the diffusion of oxygen and further corrosion.[36] In addition, the inactivation of Cr(0) may also be due to the fact that the oxidant cannot physically contact with Cr(0) inside pipe solids.

Sources of Cr in the Iron Corrosion Scales. Because Cr(0) in the iron corrosion scales was discovered as the main reservoir for oxidative Cr(VI) release in DWDSs, it is important to understand its source in the iron corrosion scales. New corrosion scales were freshly produced *ex situ* by the electrochemical corrosion using two fresh plates cut from pipe #1 and pipe #2 submerged in an electrolyte made of DI water at pH 7. Because there was no Cr(VI) in the electrolyte, the accumulation of Cr in the freshly produced corrosion scales exclusively came from the pipe material itself. Analysis showed that the freshly produced corrosion scales had very comparable zerovalent Cr(0) concentration to the naturally formed corrosion scales for pipe #1 (609 ± 18 *vs* 653 ± 40 μg/g) and pipe #2 (27 ± 1.1 *vs* 24 ± 1.9 μg/g) (Table 1). A prior study on electrochemical corrosion also showed that zerovalent

https://dx.doi.org/10.1021/acs.est.0c03922
Environ. Sci. Technol. 2020, 54, 13036−13045

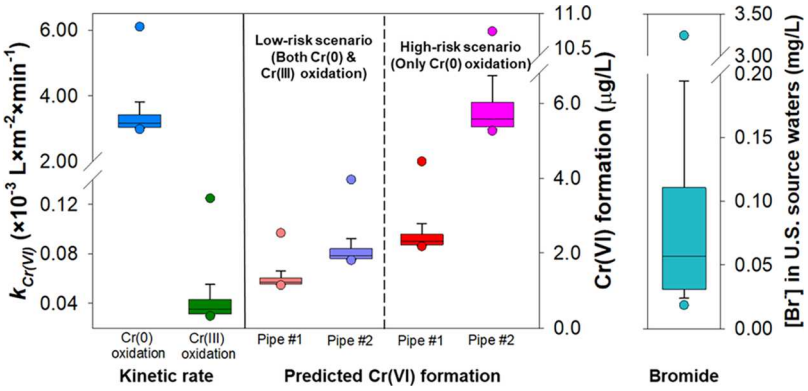

Figure 5. Predictions of percentile distributions of Cr(VI) formation rate constants and the Cr(VI) formation in drinking-water distribution systems based on statistical distributions of bromide concentration in U.S. source waters. The solid line in each box is the median value; the lower and upper box edges are the 25th and 75th percentiles. Whisker bars represent the 5th and 95th percentiles. Solid dots are the minimum and maximum values. The kinetics model simulation on Cr(VI) formation is based on the assumption that a water distribution system has the constant 0.3 mg/L chlorine residual and 100 μg/L residual Cr solids [low-risk scenario including both Cr(0) and Cr(III) solids and high-risk scenario including only Cr(0) solids] with a residence time of 2 days.

Cr(0) was observed in the surface passivation layer of iron alloys.[37] For the naturally formed iron corrosion scales, solid #1 had a Cr(0) concentration approximately 28 times higher than solid #2, and such a difference can be explained by that pipe #1 had a much higher Cr(0) concentration in its cast iron alloy composition than pipe #2 (609 ± 18 *vs* 27 ± 1.1 μg/g). In addition, reductants in the iron corrosion scales such as Fe(II) and organic matter and microbiological process can only thermodynamically reduce Cr(VI) to Cr(III).[38−41] Therefore, it is unlikely that the Cr(0) fraction in the iron corrosion scales was from the direct reduction of Cr(VI) in water. Overall, the experimental data confirmed that zerovalent Cr(0) observed in the corrosion scales originated from the zerovalent Cr fraction as a part of the cast iron alloy. Cr(III) was also found in the freshly produced corrosion scales, which was largely due to the slow oxidation of zerovalent Cr in the cast iron alloy during the electrochemical corrosion.

Furthermore, for pipe #1, total Cr accumulation was much higher in the naturally formed corrosion scales than the freshly produced corrosion scales (1333 ± 82 *vs* 652 ± 23 μg/g, Table 1). This was mainly due to the difference in Cr(III) accumulation (680 ± 42 *vs* 43 ± 5 μg/g) (Table 1) and indicated that Cr(III) cumulation in the iron corrosion scales was mainly from the source water which had very high Cr(VI) concentrations (11−24 μg/L) lasting for 5 years, that is, the age of the pipe section. The accumulation of Cr(III) solids in the iron scales from source water was also consistent with the result that the total Cr concentration in the top surface was higher than that in the bottom surface based on the detected average counts of Cr (240 *vs* 69 counts) (Figure S5). Therefore, the formation of Cr(III) in the corrosion scales was mainly due to the reduction of Cr(VI) in drinking water by chemical reductants including Fe(II) and organic matter.[15,16] In contrast, for pipe #2, because of a negligible Cr(VI) in the source water and much lower Cr concentration in the corrosion scales, the main source of Cr in the corrosion scales is the zerovalent Cr from the cast iron alloy.

Mechanisms of Chlorine Consumption by Iron Corrosion Scales. During the 7-day oxidation experiments, only a small fraction of the total oxidant consumption (<2.6 ± 0.06%) was attributed to the oxidation of Cr(0) and Cr(III) in the corrosion scales to form Cr(VI) (Figure S10). The total oxidant consumption of Cr solids was calculated based on the concentration changes of Cr(0) and Cr(III) in the suspension after 7 days of reaction and the stoichiometric molar ratio of Cr(0) and Cr(III) to the oxidation (1:3 and 2:3, respectively). The dominant reductants to react with HOCl or HOBr in the iron corrosion scales were Fe(II) and DOC in the corrosion scales. During the 7 days of oxidation reaction, the continuously decreased Fe(II) concentration in solid #1 (Figure S11) and significantly increased DOC concentrations (Figure S12) indicated that Fe(II) and organic matter could be two dominant reductions for total HOCl consumption. In order to quantify the HOCl consumption by DOC, two filtrates from suspensions of 2 g/L solid #1 and solid #2 were used to react with 200 mg/L HOCl at pH 7 for 2 h. Only at the first time point (10 min), the HOCl concentrations in the two filtrates were significantly lower than the those in the control group without DOC, indicating that the reaction between DOC and HOCl was fast and completed within 10 min. Chlorine reactions with NOM were on a timescale of minutes with very high k_{HOCl} (1.7−4.9 $L \cdot mol^{-1} \cdot s^{-1}$).[42] For solid #1, Fe(II) and DOC consumed 57 ± 4.3−64 ± 6.7 and 18 ± 1.4−38 ± 1.9% of the total HOCl, respectively, and together explained the majority of the HOCl consumption (82−95%) (Figure S13A). For solid #2, no Fe(II) was found in the initial solid, and DOC consumed 67 ± 3.9−85 ± 6.3% of the total HOCl (Figure S13B). Therefore, Fe(II) and DOC were two dominant reductants for the HOCl consumption, and higher Fe(II) and organic matter concentrations in iron corrosion scales can facilitate the HOCl consumption kinetics and diminish the Cr(VI) release.

Prediction on Cr(VI) Occurrence in DWDSs. To predict Cr(VI) release in iron-pipe dominated DWDSs, a distribution system kinetics model was established using the reaction rate constants ($k_{Cr(VI)}$) obtained from this study (details on the model in Text S2). One limitation of the prediction was that $k_{Cr(VI)}$ obtained from a high chlorine concentration (200 mg/L) was used to predict Cr(VI) formation at a low chlorine level of drinking water; thus, the prediction was largely affected by to what extend the kinetic would change under different concentrations of chlorine. However, the prediction from real iron corrosion scales can provide more accurate information for the formation of Cr(VI) in drinking water compared to that

https://dx.doi.org/10.1021/acs.est.0c03922
Environ. Sci. Technol. 2020, 54, 13036−13045

from pure Cr solids, given that the real corrosion scales had complex composition. Because of the existence of organic matter and ferrous iron as two dominant reductants and the essential low reaction activity between Cr solids and chlorine, high concentration of chlorine (200 mg/L) was used to obtain these $k_{Cr(VI)}$ in different phases in drinking water in this study. Cr(VI) formation was predicted based on statistical distributions of bromide concentration in U.S. source waters.[43] Two scenarios were considered, a low-risk scenario where the Cr solids included both Cr(0) and Cr(III) solids, and a high-risk scenario where the Cr solids were all Cr(0) solids. The formation of Cr(VI) was predicted based on a distribution system residence time of two days (Figure 5) and five days (Figure S14). Because it is impossible to accurately quantify chlorine consumption in the DWDSs because of the complexity of iron corrosion scales, a constant free chlorine residual of 0.3 mg/L relevant to drinking water was used in the model. Many states in the United States required a minimum free chlorine residual of 0.3 mg/L during water distribution.[44] The disinfection utility survey from American Water Works Association reported that systems with free chlorine residuals maintained median levels of 0.5−1.0 mg/L from entry points to maximum retention sites.[45] The free chlorine residue as a disinfectant in the drinking water can maintain an oxidizing condition and continuously form Cr(VI) through the oxidation of Cr solids in the corrosion scales. With a residence time of two days, the median Cr(VI) concentration in tap water can range between 1.2 and 1.9 μg/L under the low-risk scenario, and in contrast, the median Cr(VI) concentration in tap water can range between 2.3 and 5.6 μg/L under the high-risk scenario (Figure 5). Approximately, 85−93% of these Cr(VI) were from the oxidation of Cr(0) solids (Figure S15). When the residence time increased to 5 days, the median Cr(VI) concentration in tap water can increase to 14 μg/L at the worst scenario (Figure S14), which was higher than the previous California issued Cr(VI) drinking standard, 10 μg/L. Cr(VI) in U.S. drinking water was between 0.057 and 7.51 μg/L in 2013−2015 based on the EPA Round 4 Unregulated Contaminant Monitoring Rule Program.[46] The average Cr(VI) concentrations in Canadian and US DWDSs in 2008 to 2017 were reported to range from 0.2 to 2 μg/L.[47] Therefore, the predicted median Cr(VI) concentrations in this study were comparable to the actual Cr(VI) concentrations in drinking water. Given that the chlorine residual level (0.3 mg/L) in the modeling was approximately 3 orders of magnitude lower than that used for obtaining the $k_{Cr(VI)}$ (200 mg/L), a sensitivity analysis of the Cr(VI) concentrations at the medium bromide concentration was conducted with subjectively changing $k_{Cr(VI)}$ from 20 to 200% of the observed $k_{Cr(VI)}$ in this study. As changing $k_{Cr(VI)}$, the median Cr(VI) concentration in tap water can range between 0.25 and 3.9 μg/L under the low-risk scenario, and in contrast, the median Cr(VI) concentration in tap water can range between 0.46 and 11 μg/L under the high-risk scenario with a residence time of two days (Table S2). In the future, as more desalinated water is expected to become new water sources for drinking water sources because of water scarcity, desalinated water can introduce a bromide concentration in drinking water as high as 0.8 mg/L.[48] This level of bromide in water will lead the worst scenario to happen which is that Cr(VI) concentrations can increase to 11 μg/L with a residence time of two days and to 27 μg/L with a residence time of five days because of the catalytic effect of bromide (maximum values in Figures 5 and S14). Therefore, changing the water source from surface water to desalinated water will likely increase the risk of exposure to higher Cr(VI) in drinking water if no mitigation strategy is implemented.

Environmental Implications. This study discovered that zerovalent Cr(0) existed in cast iron corrosion scales and can oxidatively release Cr(VI) into drinking water via the oxidation of chlorine residual disinfectants. More importantly, Cr(0) had 1 to 2 orders of magnitudes higher reactivity with HOCl than other Cr(III) solids. Therefore, the Cr(VI) formation was mainly due to oxidation of the Cr(0) solid in the iron corrosion scales by HOCl in DWDSs. Furthermore, the source of Cr(0) in the iron corrosion scales was Cr(0) in the pipe material, which indicated that the Cr(0) concentration in the pipe material was the dominant factor determining the level of Cr(VI) formation in drinking water with HOCl, and the previous accumulated Cr(III) in the corrosion scales from the water source was unlikely to cause a significant level of Cr(VI) formation in drinking water. Because HOCl was very reactive with Cr(0), the mitigation of Cr(VI) occurrence in drinking water could be achieved by the use of a residual disinfectant less reactive with Cr(0). Cast iron pipe materials with high levels of alloy chromium should be used with caution in future pipe replacement for DWDSs.

The kinetics model predicts that the median Cr(VI) concentrations were 1.2−1.9 μg/L under the low-risk scenario and 2.3−5.6 μg/L under the high-risk scenario with a distribution system residence time of 2 days. Based on these predictions, an effective strategy to prevent hexavalent chromium release from iron pipe-dominant DWDSs needs to inhibit the redox reactivity of zerovalent Cr(0) in iron corrosion scales. Furthermore, more attention should be paid on bromide concentration in alternative water sources as it is a very important factor affecting the Cr(VI) levels in drinking water.

■ ASSOCIATED CONTENT

Supporting Information

The Supporting Information is available free of charge at https://pubs.acs.org/doi/10.1021/acs.est.0c03922.

Additional characterization of the iron corrosions scales (images, zero zeta potential, distribution of Fe and Cr, ferrous and DOC concentration); Cr(0) and Cr(III) recovery by different digestion methods; fitting of $k_{Cr(VI)}$; additional calculation of reduction potentials in drinking water; and modeling for the prediction of Cr(VI) concentrations in DWDSs (PDF)

■ AUTHOR INFORMATION

Corresponding Author

Haizhou Liu − *Department of Chemical and Environmental Engineering, University of California at Riverside, Riverside, California 92521, United States;* orcid.org/0000-0003-4194-2566; Phone: (951) 827-2076; Email: haizhou@engr.ucr.edu; Fax: (951) 827-5696

Authors

Cheng Tan − *Department of Chemical and Environmental Engineering, University of California at Riverside, Riverside, California 92521, United States;* orcid.org/0000-0001-5878-6542

https://dx.doi.org/10.1021/acs.est.0c03922
Environ. Sci. Technol. 2020, 54, 13036−13045

Sumant Avasarala − *Department of Chemical and Environmental Engineering, University of California at Riverside, Riverside, California 92521, United States*

Complete contact information is available at: https://pubs.acs.org/10.1021/acs.est.0c03922

Notes

The authors declare no competing financial interest.

■ ACKNOWLEDGMENTS

This research was supported by the U.S. National Science Foundation CAREER Program (CBET-1653931). We thank Samantha Ying and Michael Schaefer for the assistance on synchrotron sample preparation, Ilkeun Lee for BET analysis, and group members Henry Kouyoumdjian and Monika Madhiyan for assistance in this project at UC Riverside. We also thank Melinda Friedman at the Confluence Engineering Group and Chad Seidel at Corona Environmental Consulting for assistance in collecting the iron pipe sections. Portions of this research were carried out at the Stanford Synchrotron Radiation Lightsource, a Directorate of SLAC National Accelerator Laboratory and an Office of Science User Facility operated for the U.S. Department of Energy Office of Science by Stanford University.

■ REFERENCES

(1) Rollinson, C. L. Chromium Compounds. *The Chemistry of Chromium, Molybdenum and Tungsten*; Pergamon Press, 1973; pp 639−700.

(2) Saha, R.; Nandi, R.; Saha, B. Sources and Toxicity of Hexavalent Chromium. *J. Coord. Chem.* **2011**, *64*, 1782−1806.

(3) EPA. *National Primary Drinking Water Regulations*, Final Rule, Federal Register, 1991; Vol. *56*, pp 3536−3537.

(4) Brown, E. G.; Alexeeff, G. V. *Public Health Goals for Chemicals in Drinking*; California Environmental Protection Agency, 2011, No. Cr VI; pp 1−162.

(5) *Hexavalent Chromium in Drinking Water*; California Environmental Protection Agency, State Water Resources Board.

(6) *California Manufacturers and Technology Association and Solano County Taxpayers Association v. State Water Resources Control Board*; Superior Court of California: County of Sacramento, 2017.

(7) Chen, G.; Feng, J.; Wang, W.; Yin, Y.; Liu, H. Photocatalytic Removal of Hexavalent Chromium by Newly Designed and Highly Reductive TiO2 Nanocrystals. *Water Res.* **2017**, *108*, 383−390.

(8) Henrie, T.; Plummer, S.; Orta, J.; Bigley, S.; Gorman, C.; Seidel, C.; Shimabuku, K.; Liu, H. Full-scale Demonstration Testing of Hexavalent Chromium Reduction via Stannous Chloride Application. *AWWA Water Sci.* **2019**, *1*, No. e1136.

(9) Peng, C.-Y.; Hill, A. S.; Friedman, M. J.; Valentine, R. L.; Larson, G. S.; Romero, A. M. Y.; Reiber, S. H.; Korshin, G. V. Occurrence of Trace Inorganic Contaminants in Drinking Water Distribution Systems. *J.—Am. Water Works Assoc.* **2012**, *104*, E181−E193.

(10) Peng, C.-Y.; Ferguson, J. F.; Korshin, G. V. Effects of Chloride, Sulfate and Natural Organic Matter (NOM) on the Accumulation and Release of Trace-Level Inorganic Contaminants from Corroding Iron. *Water Res.* **2013**, *47*, 5257−5269.

(11) Chebeir, M.; Chen, G.; Liu, H. Emerging Investigators Series: Frontier Review: Occurrence and Speciation of Chromium in Drinking Water Distribution Systems. *Environ. Sci.: Water Res. Technol.* **2016**, *2*, 906−914.

(12) Chebeir, M.; Liu, H. Kinetics and Mechanisms of Cr(VI) Formation via the Oxidation of Cr(III) Solid Phases by Chlorine in Drinking Water. *Environ. Sci. Technol.* **2016**, *50*, 701−710.

(13) Chebeir, M.; Liu, H. Oxidation of Cr(III)-Fe(III) Mixed-Phase Hydroxides by Chlorine: Implications on the Control of Hexavalent Chromium in Drinking Water. *Environ. Sci. Technol.* **2018**, *52*, 7663−7670.

(14) Singh, R. *Applied Welding Engineering: Processes, Codes, and Standards*, 2nd ed, 2015; p 74.

(15) Peng, C.-Y.; Korshin, G. V.; Valentine, R. L.; Hill, A. S.; Friedman, M. J.; Reiber, S. H. Characterization of Elemental and Structural Composition of Corrosion Scales and Deposits Formed in Drinking Water Distribution Systems. *Water Res.* **2010**, *44*, 4570−4580.

(16) Mcneill, L. S.; Edwards, M. Iron Pipe Corrosion in Distribution Systems. *J.—Am. Water Works Assoc.* **2001**, *93*, 88−100.

(17) Bichsel, Y.; Von Gunten, U. Oxidation of Iodide and Hypoiodous Acid in the Disinfection of Natural Waters. *Environ. Sci. Technol.* **1999**, *33*, 4040−4045.

(18) Gallard, H.; von Gunten, U. Chlorination of Phenols: Kinetics and Formation of Chloroform. *Environ. Sci. Technol.* **2002**, *36*, 884−890.

(19) Frateur, I.; Deslouis, C.; Kiene, L.; Levi, Y.; Tribollet, B. Free Chlorine Consumption Induced by Cast Iron Corrosion in Drinking Water Distribution Systems. *Water Res.* **1999**, *33*, 1781−1790.

(20) Torrice, M. How Lead Ended up in Flint's Tap Water. *Chem. Eng. News* **2016**, *94*, 26−29.

(21) Edwards, M.; Triantafyllidou, S.; Best, D. Elevated Blood Lead in Young Children Due to Lead-Contaminated Drinking Water: Washington, DC, 2001−2004. *Environ. Sci. Technol.* **2009**, *43*, 1618−1623.

(22) National Research Council of the National Academies. *Water Reuse: Potential for Expanding the Nation's Water Supply through Reuse of Municipal Wastewater*; The National Academies Press: Washington, DC, 2012.

(23) Sarin, P.; Snoeyink, V. L.; Lytle, D. A.; Kriven, W. M. Iron Corrosion Scales: Model for Scale Growth, Iron Release, and Colored Water Formation. *J. Environ. Eng.* **2004**, *130*, 364−373.

(24) Hansel, C. M.; Wielinga, B. W.; Fendorf, S. Structural and Compositional Evolution of Cr/Fe Solids after Indirect Chromate Reduction by Dissimilatory Iron-Reducing Bacteria. *Geochim. Cosmochim. Acta* **2003**, *67*, 401−412.

(25) Liu, H.; Korshin, G. V.; Ferguson, J. F. Investigation of the Kinetics and Mechanisms of the Oxidation of Cerussite and Hydrocerussite by Chlorine. *Environ. Sci. Technol.* **2008**, *42*, 3241−3247.

(26) Orta, J.; Patton, S.; Liu, H. Bromide-Assisted Catalytic Oxidation of Lead(II) Solids by Chlorine in Drinking Water Distribution Systems. *Chem. Commun.* **2017**, *53*, 8695−8698.

(27) Allard, S.; Fouche, L.; Dick, J.; Heitz, A.; Von Gunten, U. Oxidation of Manganese(II) during Chlorination: Role of Bromide. *Environ. Sci. Technol.* **2013**, *47*, 8716−8723.

(28) USEPA. *Method 3050B Acid Digestion of Sediments, Sludges and Soils, Revision 2*; Environmental Protection Agency: Washington, USA, 1996; pp 3−5.

(29) Bruno, L. *Standard Methods for the Examination of Water and Wastewater*, 23rd ed.; American Public Health Association, 2017; Vol. *53*.

(30) Zhang, L.; Jun, Y.-S. The Role of Fe-Bearing Phyllosilicates in DTPMP Degradation under High-Temperature and High-Pressure Conditions. *Environ. Sci. Technol.* **2018**, *52*, 9522−9530.

(31) Jain, A.; Raven, K. P.; Loeppert, R. H. Arsenite and Arsenate Adsorption on Ferrihydrite: Surface Charge Reduction and Net OH-Release Stoichiometry. *Environ. Sci. Technol.* **1999**, *33*, 1179−1184.

(32) Zhao, Z.; Jia, Y.; Xu, L.; Zhao, S. Adsorption and Heterogeneous Oxidation of As(III) on Ferrihydrite. *Water Res.* **2011**, *45*, 6496−6504.

(33) Friedman, M. J.; Hill, A. S.; Reiber, S. H.; Valentine, R. H.; Korshin, G. V. *Assessment of Inorganics Accumulation in Drinking Water System Scales and Sediments*; Water Research Foundation, 2010.

(34) Fendorf, S. E.; Li, G. Kinetics of Chromate Reduction by Ferrous Iron. *Environ. Sci. Technol.* **1996**, *30*, 1614−1617.

(35) Dai, C.; Zuo, X.; Cao, B.; Hu, Y. Homogeneous and Heterogeneous (Fex, Cr1-x)(OH)3 Precipitation: Implications for Cr Sequestration. *Environ. Sci. Technol.* **2016**, *50*, 1741−1749.
(36) Wallwork, G. R. The Oxidation of Alloys. *Rep. Prog. Phys.* **1976**, *39*, 401−485.
(37) Bera, S.; Rangarajan, S.; Narasimhan, S. V. Electrochemical Passivation of Iron Alloys and the Film Characterisation by XPS. *Corros. Sci.* **2000**, *42*, 1709−1724.
(38) Li, N.; Li, W.; Fu, F. Removal of Chromium(VI) by MnFe2O4 and Ferrous Ion: Synergetic Effects and Reaction Mechanism. *Environ. Sci. Pollut. Res.* **2019**, *26*, 30498−30507.
(39) Chiu, C.-C.; Cheng, C.-J.; Lin, T.-H.; Juang, K.-W.; Lee, D.-Y. The Effectiveness of Four Organic Matter Amendments for Decreasing Resin-Extractable Cr(VI) in Cr(VI)-Contaminated Soils. *J. Hazard. Mater.* **2009**, *161*, 1239−1244.
(40) Al Hasin, A.; Gurman, S. J.; Murphy, L. M.; Perry, A.; Smith, T. J.; Gardiner, P. H. E. Remediation of Chromium(VI) by a Methane-Oxidizing Bacterium. *Environ. Sci. Technol.* **2010**, *44*, 400−405.
(41) Caravelli, A. H.; Giannuzzi, L.; Zaritzky, N. E. Reduction of Hexavalent Chromium by Sphaerotilus Natans a Filamentous Micro-Organism Present in Activated Sludges. *J. Hazard. Mater.* **2008**, *156*, 214−222.
(42) Westerhoff, P.; Chao, P.; Mash, H. Reactivity of Natural Organic Matter with Aqueous Chlorine and Bromine. *Water Res.* **2004**, *38*, 1502−1513.
(43) Wilson, J. M.; Wang, Y.; Vanbriesen, J. M. Sources of High Total Dissolved Solids to Drinking Water Supply in Southwestern Pennsylvania. *J. Environ. Eng.* **2014**, *140*, b4014003.
(44) National Primary Drinking Water Regulations. *Announcement of the Results of EPA's Review of Existing Drinking Water Standards and Request for Public Comment And/or Information on Related Issues*; EPA, Federal Register, 2017; Vol. *82*, pp 3518−3552.
(45) Routt, J.; Mackey, E.; Noack, R.; Passantino, L.; Connell, G.; Sacco, A.; Koch, D.; Cosman, J.; Swaim, P.; Whitby, E.; DeGraca, A.; Nieminski, E.; Malley, J.; Via, S.; Bess, J.; Cleveland, C.; Dussert, B.; Dwyer, T.; Ertas, T.; Fontaine, N.; Herrington, R.; Grenne, D.; Haas, C.; Johnson, C.; Liu, S.; Mutti, D.; Mutoti, I.; Oxner, K.; Peters, D.; Posy, P.; Rindal, D.; Rivera, S.; Smith, C.; Winsor, W.; Valade, M. Committee Report: Disinfection Survey, Part 1 - Recent Changes, Current Practices, and Water Quality. *J.—Am. Water Works Assoc.* **2008**, *100*, 76−91.
(46) United States Environmental Protection Agency. *Unregulated Contaminant Monitoring Rule 3 (UCMR 3)*, 2015.
(47) Moffat, I.; Martinova, N.; Seidel, C.; Thompson, C. M. Hexavalent Chromium in Drinking Water. *J.—Am. Water Works Assoc.* **2018**, *110*, E22−E35.
(48) Liu, H.; Schonberger, K. D.; Korshin, G. V.; Ferguson, J. F.; Meyerhofer, P.; Desormeaux, E.; Luckenbach, H. Effects of Blending of Desalinated Water with Treated Surface Drinking Water on Copper and Lead Release. *Water Res.* **2010**, *44*, 4057−4066.

https://dx.doi.org/10.1021/acs.est.0c03922
Environ. Sci. Technol. 2020, 54, 13036−13045